Thompson Alexander, James (Orcid ID: 0000-0002-8037-5990)
Skinner Christopher, Bryan (Orcid ID: 0000-0002-8105-8698)
Poulsen Christopher J. (Orcid ID: 0000-0001-5104-4271)
Zhu Jiang (Orcid ID: 0000-0002-0908-5130)

Modulation of mid-Holocene African rainfall by dust aerosol direct and indirect effects

Alexander J. Thompson[1], Christopher B. Skinner[1,2], Christopher J. Poulsen[1], and Jiang Zhu[1]

[1]Department of Earth and Environmental Sciences, University of Michigan, Ann Arbor, Michigan, USA, [2]Department of Environmental, Earth and Atmospheric Sciences, University of Massachusetts Lowell, Lowell, MA, USA

Corresponding author: Alexander J. Thompson (alexjt@umich.edu)

Key Points:

- Changes in direct dust aerosol effects from reduced mid-Holocene Saharan dust loading increase convective rainfall in northern Africa.
- Changes in indirect dust aerosol effects weaken total precipitation increases by limiting stratiform rainfall, particularly in the Sahel.

This is the author manuscript accepted for publication and has undergone full peer review but has not been through the copyediting, typesetting, pagination and proofreading process, which may lead to differences between this version and the Version of Record. Please cite this article as doi: 10.1029/2018GL081225

- The African rainfall response to total dust aerosol effects is lower than a previous study and substantially less than vegetation forcing.

Abstract

Climate model simulations of the mid-Holocene (MH) consistently underestimate northern African rainfall for reasons not fully understood. While most models incorporate orbital forcing and vegetation feedbacks, they neglect dust reductions associated with greater vegetation cover. Here we simulate the MH climate response to reduced Saharan dust using CESM CAM5-chem, which resolves direct and indirect dust aerosol effects. Direct aerosol effects increase Saharan and Sahel convective rainfall by ~16% and 8%. In contrast, indirect aerosol effects decrease stratiform rainfall, damping the dust-induced total rainfall increase by ~13% in the Sahara and ~59% in the Sahel. Sensitivity experiments indicate the dust-induced precipitation anomaly in the Sahara and Sahel (0.27 and 0.18 mm day^{-1}) is smaller than the anomaly from MH vegetation cover (1.19 and 1.08 mm day^{-1}). Although sensitive to dust radiative properties, SSTs, and indirect aerosol effect parameterization, our results suggest that dust reductions had competing effects on MH African rainfall.

Plain Language Summary

Six thousand years ago, changes in Earth's orbit led to greater summer season solar radiation over northern Africa. The increase in energy resulted in higher rainfall amounts, widespread vegetation, and reduced dust aerosols over regions that today are desert. In this study we use a climate model, CESM CAM5-chem, that accounts for the ways dust aerosols interact with sunlight and cloud droplets to examine how the reduction in Saharan dust during this past humid time affected rainfall. When dust aerosols are reduced in the model, more sunlight reaches the surface, the Sahara warms, and convective rainfall from the West African Monsoon increases. However, through dust-cloud droplet interactions, the same reduction in dust decreases non-convective rainfall, which is less prevalent during the monsoon season but still important, and thus dampens the total rainfall increase. Overall, dust reduction leads to a rainfall response that is dependent on rainfall type. Lastly, we compare the rainfall response of reducing dust to that of increasing vegetation cover and find that while important, the response from dust is considerably weaker.

1 Introduction

Northern Africa has experienced wet and dry phases fluctuating on orbital timescales since at least the late Miocene (deMenocal, 1995; Zhang et al., 2014). At the end of the African

Humid Period (AHP; ~14.8 to 5.5 ka BP), the most recent wet phase, portions of the Sahara transitioned from a largely vegetated landscape to desert within only a few centuries (deMenocal et al., 2000; Tierney et al., 2017). Proxy records and general circulation models provide evidence that Quaternary orbital-scale humid periods, including the early to mid-Holocene AHP, are linked to precession-driven enhancements of boreal summer insolation, which strengthen monsoonal flow and increase rainfall across northern Africa (deMenocal, 1995; Kutzbach, 1981; Tjallingii et al., 2008; Tuenter et al., 2007). Insolation changes alone, however, are insufficient to explain the climate and ecological changes inferred from AHP proxies (Joussaume et al., 1999). The latest mid-Holocene (MH; 6 ka BP) climate model simulations from Paleoclimate Modelling Intercomparison Project Phase 3 (PMIP3), which, by design, include orbital insolation changes but neglect biogeophysical changes in northern Africa, underestimate AHP precipitation by as much as 400 mm $year^{-1}$ (Perez-Sanz et al., 2014).

The discrepancy between proxy-derived and climate model estimates of rainfall has spurred investigation of the land-atmosphere interactions that shaped northern African hydroclimate change (e.g., Braconnot et al., 1999; Charney, 1975; Claussen & Gayler, 1997; Claussen et al., 1999; Vamborg et al., 2014). Several lines of proxy evidence indicate that steppe, savanna, and shrub vegetation reached up to 31°N (Hoelzmann et al., 1998; Jolly et al. 1998; Shanahan et al., 2015; Tierney et al., 2017). By reducing Saharan surface reflectance and enhancing evapotranspiration, expanded vegetation cover modified the local surface energy balance and increased both moist static energy and rainfall (Charney, 1975; Charney et al., 1975; Eltahir, 1998). Climate modeling studies have confirmed vegetation as a positive feedback on precessional forcing to enhance AHP precipitation (Boos & Korty, 2016; Brovkin et al., 1998; Knorr & Schnitzler, 2006; Levis et al., 2004; Patricola & Cook, 2007; Skinner & Poulsen, 2016). However, even after accounting for vegetation expansion, climate models do not adequately simulate the intensity and northward extent of rainfall inferred from Saharan proxy records (Brostrom et al., 1998; Hoelzmann et al., 1998; Tierney et al., 2017).

Vegetation also indirectly impacts northern African climate through its control on dust mobilization. During the AHP, vegetation in the Sahara resulted in dust aerosol emissions two to three times lower than today (deMenocal et al., 2000; Egerer et al., 2016; McGee et al., 2013). This decrease in dust is postulated to have impacted AHP precipitation through direct, indirect, and semi-direct dust aerosol effects (Pausata et al., 2016; Perlwitz & Miller, 2010; Williams et al., 2016). Direct aerosol effects describe the scattering and absorption of radiation by aerosols (Ghan et al., 2012). Indirect aerosol effects account for alterations to cloud optical properties and precipitation efficiency, through changes in droplet number concentration and size, that occur when aerosols nucleate cloud droplets (Ghan et al., 2013; Xie et al., 2017). Semi-direct aerosol effects include the response of clouds to radiative heating of atmospheric aerosols (Ghan et al., 2012; Grassl, 1975). Over present-day northern Africa, direct dust aerosol effects impact rainfall variability by influencing surface warming and, by extension, deep convection (Huang et al., 2009). The response of rainfall to dust indirect aerosol effects is less understood; studies have shown that Saharan dust aerosols nucleate ice clouds, and liquid clouds to a lesser extent, and

suppress rainfall in northern Africa (DeMott et al., 2003; Huang et al., 2009; Rosenfeld et al., 2001; Sassen et al., 2003).

Vegetation-driven dust reductions on AHP precipitation have received relatively little attention. To date, most model simulations, including those from PMIP3, specify preindustrial (PI) dust loading (Braconnot et al., 2011; Taylor et al., 2012). Using a model that only resolves direct aerosol effects, Pausata et al. (2016) accounted for changes in MH vegetation cover and the associated dust reduction and found that a reduced dust load enhanced local rainfall by as much as 2.5 mm day^{-1} over the Sahara and shifted the West African Monsoon (WAM) northwards. With the same model, Messori et al. (2018) showed that increased moisture recycling was a key driver of the rainfall response to reduced atmospheric dust load. However, the potential role of indirect aerosol effects, which have at least equal global radiative forcing (Myhre et al., 2013), on AHP precipitation, have never been explored.

Here, we investigate the role of dust on MH African climate with the CESM CAM5-chem model, which includes both direct and indirect aerosol effects. For context, we also compare the role of dust in shaping MH African climate with that of orbital forcing and vegetation cover.

2 Model Experiments and Methods

We employed the Community Atmosphere Model version 5 with tropospheric chemistry (CAM5-chem) coupled to the Community Land Model version 4.0 (CLM4.0) (Neale et al., 2012; Oleson et al., 2010). The atmosphere (CAM5-chem) and land (CLM4.0) models are run with a grid resolution of 0.9° latitude × 1.25° longitude. CAM5-chem contains 30 vertical levels; CLM4.0 contains 15 soil-column layers. CAM5-chem is suited for studies involving atmospheric aerosols because it explicitly predicts ice and mixed-phase immersion, deposition, and contact nucleation by dust aerosols for stratiform clouds; these explicit nucleation processes are absent for convective clouds (Neale et al., 2012; Tilmes et al., 2015). In general, the addition of microphysics parameterizations related to aerosol indirect effects lead to better simulation of regional rainfall (Lin et al., 2018). Sagoo and Storelvmo (2017) show that increased dust leads to enhanced ice nucleation and suppressed tropical rainfall in CAM5, consistent with observations (e.g., Rosenfeld et al., 2001). Over Africa, the model reasonably simulates modern precipitation, including the seasonal cycle and total rainfall amount (Skinner and Poulsen, 2016). A description of aerosol properties in CAM5-chem can be found in Text S1.

In CLM4.0, vegetation leaf area index (LAI) and stem area index (SAI) are prescribed for each plant functional type (PFT) and vary monthly. Dust is mobilized diagnostically from the land surface by the Dust Entrainment and Deposition (DEAD) model from Zender et al. (2003). We follow Skinner and Poulsen (2016) and use prescribed monthly-varying MH sea surface temperatures (SSTs) calculated by adding the SST anomalies from the fully coupled CCSM4 mid-Holocene 6 ka simulation (Gent et al., 2011; Taylor et al., 2012) to average monthly SSTs from years 1870 to 1890 of the merged Hadley-OI observation data set (Hurrell et al., 2008). In

order to equilibrate the atmosphere model with the land model, each simulation is run for 35 years, with the last 30 years used in analysis, following Skinner and Poulsen (2016).

We ran a total of six CAM5-chem simulations to isolate the individual and combined contributions of orbital forcing, vegetation cover, soil albedo, and dust emissions on MH African climate (Table 1). Our control simulations, *PI Control* and *MH Control*, have orbital parameters, greenhouse gas concentrations, SSTs, and land surface parameters, including soil albedo and vegetation cover, set to PI and MH values, respectively (Table S1). Our prescription of MH vegetation included changes to PFT percentage and values of LAI (Table S2) (Davies et al., 2015; Hoelzmann et al., 1998; Levis et al., 2004; Pausata et al., 2016). MH values for dry and saturated soil albedo are prescribed separately from vegetation (Table S2), and soil texture is not changed from PI values in any simulation. In CLM4.0, dust mobilization is prohibited when leaf and stem area values (LAI+SAI) exceed 0.3 (Oleson et al., 2010). In *MH Control*, northern African LAI+SAI exceeded this threshold year-round preventing dust mobilization over the prescribed land surface. A comparison between *MH Control* and *PI Control* provides an estimate of the total climate change between the MH and PI time periods (Figures S2, S3).

Sensitivity experiments were conducted to isolate the individual impacts of dust loading (*MH HighDust*), orbital forcing (*MH Orbital*), MH vegetation (*MH DesertVeg*), and MH soil albedo (*MH DesertSoil*). The *MH HighDust* simulation is identical to *MH Control* except the vegetational control on dust mobilization was removed. Thus, *MH HighDust* allowed dust emissions to occur in the presence of a vegetated Sahara (Table 1). *MH Orbital* is identical to *PI Control* except for its specified MH orbit. *MH DesertVeg* and *MH DesertSoil* are both identical to *MH Control* except *MH DesertVeg* includes PI Saharan vegetation (i.e. a desert Sahara) and *MH DesertSoil* contains PI soil albedo values underneath a vegetated MH Sahara (Table 1). We prohibited dust mobilization in *MH DesertVeg* despite the simulation's absence of MH vegetation.

A description of the offline radiative transfer calculation method used to isolate the direct aerosol effect associated with Saharan dust can be found in Text S2. We assessed the statistical significance of changes between simulations at the 95% confidence level using the Student's *t* test with the assumption of different population variances. Given the considerably larger changes in dust loading over the Sahara (20–31°N, 20°W–30°E) in our experiments (Figure 1a), we focus primarily on climate changes in this region. We provide detailed analyses of the Sahel (10–20°N, 15°W–30°E) climate response in Table 1 and the Supplemental Information.

3 Results

3.1 Saharan Dust Mobilization

Simulated dust aerosol optical depth (AOD) varies substantially between simulations due to the dependence of dust mobilization on vegetation and wind speed (Table 1, Figure S4; Zender et al., 2003). For *MH HighDust*, the average monsoon season (JJAS: June, July, August, September) dust AOD over the Sahara is 123% higher than *PI Control* (Table 1). High dust

AOD occurs because of the strong enhancement of monsoon flow associated with the combined influences of greater MH summer insolation and a lower surface albedo (Figures S3, S4). In *MH Control*, *MH DesertSoil*, and *MH DesertVeg*, Saharan dust mobilization is prohibited because the prescribed vegetation LAI+SAI values exceed 0.3; however, the Sahara dust AOD in these simulations is not strictly zero with values of ~0.2–0.3, representing trace dust emissions originating from distant source regions (Table 1, Figure S4). Differences between *MH Control* and *MH HighDust* isolate the simulated climate response to a 98% reduction in JJAS dust AOD over the Sahara (Figure 1a). In *MH Orbital*, dust AOD is 12% higher than *PI Control* due to slightly enhanced monsoon flow and greater convergence along the intertropical front from the MH increase in summer insolation (Figures S3, S4). Averages of single-scatter albedo over the Sahara, which illustrate the absorption properties of the dust layer, are in Table S3.

3.2 Direct Dust Aerosol Effects

The direct aerosol effects associated with a reduction in Saharan dust in CAM5-chem (*MH Control – MH HighDust*) act to increase net surface and top-of-the-atmosphere (TOA) shortwave radiation and surface temperature throughout the Sahara, which lead to increased convective rainfall. Our offline radiation calculation indicates that JJAS Saharan-average net downward shortwave radiation increases by 67.4 W m^{-2} and 13.7 W m^{-2} at the surface and TOA, respectively, due to reduction in backscattering from the removal of dust (Figure 1b, Table S4, Figure S5). Direct aerosol effects warm the Sahara partly by enhanced TOA forcing, which couples upper tropospheric temperatures with the surface via convective mixing (Figure 1c; Miller et al., 2014). The excess energy input at the surface is partitioned into positive sensible and latent heat fluxes (Figure S5), increasing convection and convective cloud cover throughout the atmospheric column (Figure 1d). The enhanced convective cloud cover contributes to the 15.9% increase in JJAS convective rainfall (from 1.95 to 2.26 mm day^{-1}) over the Sahara (Table 1, Figure 1e), contributing substantially to the total precipitation increase of 11.9% (from 2.27 to 2.54 mm day^{-1}) (Table 1, Figure 1f). Likewise, JJAS convective rainfall increases by 7.9% in the Sahel (from 5.47 to 5.90 mm day^{-1}), contributing to a total rainfall increase of 2.4% (from 7.44 to 7.62 mm day^{-1}) (Table 1). This result agrees qualitatively with previous modeling studies that find increased northern African precipitation in response to enhanced direct radiative forcing from a reduced dust load (Huang et al., 2009; Pausata et al., 2016). We note that the magnitude of rainfall response has been found to be sensitive to details of the radiative properties of dust with stronger absorbing dust leading to greater monsoonal rainfall (Hopcroft & Valdes, 2018; Miller et al., 2004a; Strong et al., 2015).

3.3 Indirect Dust Aerosol Effects

Our dust sensitivity experiment further demonstrates that the indirect aerosol effects associated with reduced Saharan dust loading act to decrease stratiform rainfall over the Sahara and Sahel, and thus dampen the rainfall increase from direct dust aerosol effects. When JJAS dust is reduced, the average in-cloud droplet number concentration decreases and in-cloud

droplet radius increases throughout much of the atmospheric column (Figure 2a-d, Figure S6c-f), consistent with expected indirect aerosol effects (Ghan et al., 2013; Xie et al., 2017) and previous research in northern Africa (DeMott et al., 2003; Rosenfeld et al., 2001). As a result of the altered stratiform cloud microphysics, Saharan- and Sahel-average JJAS stratus cloud fraction decreases through nearly the entire atmospheric column (Figure 2e, Figure S6b). These decreases in stratus cloud cover contribute to a 12.5% reduction (0.32 to 0.28 mm day^{-1}) in JJAS stratiform rainfall over the Sahara (Table 1, Figure 2f). In the Sahel, a larger magnitude reduction in stratiform rainfall (from 1.97 to 1.72 mm day^{-1}) occurs due to the higher stratus cloud cover there (Table 1, Figures 2e-f, S6b). The stratiform rainfall difference due to dust in the Sahel is more than six times higher (0.25 mm day^{-1} vs. 0.04 mm day^{-1}); however, the percent reduction is similar in both regions (-12.7% vs. -12.5%) (Table 1).

While the dominant type of precipitation over northern Africa is convective rainfall, which comprises over 70% of total rainfall in each simulation (Table 1), the decrease in stratiform rainfall, stemming from indirect aerosol effects, counteracts the increase in convective rainfall and thus dampens the total precipitation increase by 13.1% over the Sahara and 58.6% over the Sahel (Table 1). Overall, total JJAS precipitation increases by 11.9% (0.27 mm day^{-1}) and 2.4% (0.18 mm day^{-1}) over the Sahara and Sahel, respectively, resulting from 0.31 mm day^{-1} and 0.43 mm day^{-1} increases in convective rainfall and 0.04 mm day^{-1} and 0.25 mm day^{-1} decreases in stratiform rainfall (Table 1, Figure 1e-f, Figure 2f).

3.4 Comparison of Dust, Orbital, and Vegetation Effects

To quantify the MH northern African rainfall response to orbital forcing and vegetation, we calculate the change in total JJAS precipitation for each simulation relative to *PI Control*. *MH Control* exhibits the largest Saharan rainfall increase and northward expansion with 2.28 mm day^{-1} higher rainfall and a northern WAM limit 9.4° further north than *PI Control* (Text S3; Table 1). The three simulations with MH vegetation (*MH Control*, *MH HighDust*, and *MH DesertSoil*) exhibit rainfall and northern WAM limit increases more than double that from orbital forcing alone (Table 1). The increase in Saharan-average JJAS rainfall due to dust (direct and indirect aerosol effects combined) is 0.27 mm day^{-1} (0.18 mm day^{-1} in the Sahel), while the response due solely to vegetation is 1.19 mm day^{-1} (1.08 mm day^{-1} in the Sahel) (Table 1; *MH Control – MH HighDust* compared with *MH Control – MH DesertVeg*). Though much less than the response to vegetation, the Saharan precipitation response to dust forcing alone is not insubstantial and is comparable to that from orbital forcing (0.36 mm day^{-1}) (Table 1; *MH Orbital – PI Control*).

4 Discussion

Our results indicate that a reduced Saharan dust load during the humid MH had complex and competing influences on cloud properties and precipitation in northern Africa. We find that changes in direct dust aerosol effects increase MH African precipitation, in agreement with previous studies (e.g., Pausata et al., 2016; Williams et al., 2016), and that changes in indirect

dust aerosol effects decrease stratiform rainfall, dampening the overall increase in MH African precipitation. Although our experiments cannot directly differentiate direct and indirect aerosol effects of dust in CAM5-chem, we show that direct dust aerosol effects lead to enhanced net radiation, which increases convective clouds and rainfall (Figure 1), whereas the reductions in stratus clouds and stratiform rainfall likely result from the cloud droplet changes associated with indirect dust aerosol effects (Figure 2) because indirect aerosol effects are predicted for stratiform clouds, but are absent for convective clouds.

While we cannot rule out that aerosol absorption or surface warming due to direct dust aerosol effects played a role in decreasing stratiform cloud cover (Figure 2e) (Bretherton, 2015; Perlwitz & Miller, 2010), indirect aerosol effects likely play a larger role in driving the decrease. Aerosol absorption over the Sahara shows large decreases of up to 80% from the surface to ~500 hPa when dust is reduced (Figure S7), which is inconsistent with the stratiform cloud reduction profile at these levels. The changes in indirect aerosol effects (Figure 2a-d) are more consistent with the low- and high-level decreases in stratiform cloud cover and insignificant changes at ~600 hPa. Likewise, we tested the response to surface warming in our simulations by performing a sensitivity experiment with darker soil (*MH Control – MH DesertSoil*) to simulate the response of stratus clouds to land surface warming (Figure S8). The darkened soil produces surface warming of 0.2°C over grasslands in the northeastern Sahara and a slight (non-significant) increase in stratus cloud cover in that region (Figure S8). Based on these results, we argue that, at the very least, aerosol absorption and surface warming are not driving the stratiform cloud reductions to a greater degree than indirect aerosol effects.

Modeling results on the response of African monsoonal rainfall to MH dust forcing differ quantitatively here from previous studies (e.g., Pausata et al., 2016). However, the exact reasons for the discrepancy are difficult to address, as previous studies employed different climate models with different physical parameterizations and used distinct experiment designs. We highlight that these differences, especially prescription of SST and the corresponding absence of ocean surface energy balance, require us to make a qualitative comparison between our results and those of Pausata et al. (2016). Coordinated climate model experiments using multiple models are needed to further assess these differences; however, there are several observations we can make.

In our study, the average dust-induced MH Saharan precipitation anomaly is 0.27 mm day^{-1} (with local maxima up to 1.5 mm day^{-1}) (Table 1, Figure 1f), while Pausata et al. (2016) simulates anomalies of 0.5 to 2.5 mm day^{-1} (an average Saharan value was not given). We attribute a portion of this discrepancy to the addition of indirect aerosol effects in our model, which are lacking in EC-Earth. The total dust-induced Saharan rainfall increase in our study (11.9% in the Sahara and 2.4% in the Sahel) includes changes to both dust direct (impacting convective rainfall) and indirect (impacting stratiform rainfall) aerosol effects. If we instead only consider changes in direct aerosol effects (i.e. convective rainfall), our simulations exhibit a 13.7% increase in Saharan rainfall (5.8% in the Sahel) (Table 1). Thus, inclusion of indirect aerosol effects dampens the overall Saharan precipitation increase from reduced dust by 13.1%

(58.6% in the Sahel) (Table 1). If this damping from indirect aerosol effects holds in EC-Earth, its dust-induced rainfall anomaly would be smaller and produce better inter-model agreement.

Atmosphere-ocean coupling may also account for a portion of the dust-induced rainfall response discrepancy across climate models. Our dust-induced MH precipitation anomaly is likely sensitive to the uncertainties in ocean coupling and may differ with a dynamic ocean. EC-Earth from Pausata et al. (2016) includes dynamic SSTs that adjust to changes in atmospheric dust loading (Hazeleger et al., 2010; Madec, 2008). SSTs warm, in response to reduced dust, and increase WAM rainfall (Pausata et al. 2016). In the absence of indirect dust aerosol effects, however, the SST warming may be overestimated (Sagoo & Storelvmo, 2017). Our simulations have fixed SSTs, which, by nature, cannot respond to changes in dust loading. This potentially limits the magnitude of rainfall increase because the reduction in net surface radiation is not compensated by reduced evaporation (Miller et al., 2004b; Yoshioka et al., 2007). However, SST prescription likely cannot explain the entire discrepancy. Williams et al. (2016) shows that the increase in African rainfall due to the SST response to reduced dust cannot account for the ~1–2 mm day^{-1} difference between CAM5-chem and EC-Earth.

Physical parameterization of clouds and rainfall also likely contributes to the discrepancy. Generally, differences in convective and microphysics parameterization schemes have been shown to modify the rainfall response to dust aerosols (Solmon et al., 2012; Huang et al., 2018). More specifically, CAM5-chem differs from EC-Earth in that it utilizes a diagnostic microphysics scheme instead of a prognostic scheme (Forbes et al., 2011; Neale et al., 2012), which may account for a portion of its reduced rainfall anomaly. Analysis by Xie et al. (2012) suggests that CAM5 (with a diagnostic microphysics scheme) predicts ~2 mm day^{-1} less rainfall over equatorial Africa than CAM4 (with a prognostic microphysics scheme). A comparison of the rainfall response to vegetation in CAM5-chem and EC-Earth suggests a similar difference in rainfall sensitivity may exist between these models. EC-Earth ($MH_{GS2\text{-}PD} - MH_{CNTL}$ in Pausata et al., 2016) exhibits a larger rainfall increase (> 6 mm day^{-1}) than CAM5-chem (*MH HighDust* – *MH Orbital*) (< 5 mm day^{-1}), despite exhibiting a similar Saharan surface albedo change (within 0.05) (Figure S9). However, this is not a clean comparison because our experiment changes dust AOD, while Pausata et al. (2016) does not. Yet, the larger response in EC-Earth may suggest larger rainfall sensitivity in the model.

While the total precipitation response to MH dust, and especially indirect aerosol effects, is fairly small in CAM5-chem, our results confirm that inclusion of MH dust changes improves AHP model-data comparisons (Figure S10). However, given the failure of our most realistic MH simulation (*MH Control*) to fully enhance MH northern African rainfall to 31°N, we suggest that either 1) additional mechanisms are required beyond inclusion of the MH reduction in Saharan dust in AHP simulations, or 2) the hydroclimate responses to existing forcings and feedbacks in CAM5-chem are underestimated. With our analysis, we have identified for the first time a role of indirect dust aerosol effects in shaping MH northern African precipitation change. Our results suggest that models that do not incorporate indirect dust aerosol effects likely overestimate the dust contribution to enhanced precipitation, with the caveat that CAM5-chem neglects indirect

aerosol effects in convective clouds, including ice nucleation, which may have potentially important impacts (Hoose et al., 2008; Vergara-Temprado et al., 2017). Future work should seek to calculate dust-induced MH precipitation anomalies with the full range of indirect aerosol effects.

5 Conclusion

We use CESM CAM5-chem, a climate model that resolves direct and indirect aerosol effects, to investigate the impact of dust on MH African climate. We find that when dust is reduced over the Sahara, the associated direct dust aerosol effects lead to a positive radiative forcing at the surface and TOA, warmer surface temperatures, increased convection, and increased convective rainfall. Due to the overwhelmingly convective nature of northern Africa during the MH monsoon season, the increase in convective rainfall ultimately supports a ~12% increase in total Saharan precipitation (2.4% in the Sahel). A concurrent decrease in indirect dust aerosol effects, which impact stratiform microphysics in CAM5-chem, counteracts the increase in convective rainfall. The reduction in Saharan dust loading leads to reduced number concentrations and increased size of cloud droplets. Consequently, stratiform rainfall decreases, which dampens the total Saharan precipitation response to dust by ~13% (58.6% in the Sahel). The results indicate that the inclusion of indirect dust aerosol effects has a secondary but important influence on MH African precipitation amount and characteristics (stratiform vs. convective). This work also has implications for future climate in the Sahel, as it improves our understanding of the vegetation-dust-precipitation feedback, which may be key in shaping future precipitation as land use change and continued warming alter vegetation and dust mobilization in northern Africa (Evan et al., 2016; Yu et al., 2016; Zhu et al., 2016). Though the sign of the overall precipitation response to reduced dust in CAM5-chem matches that in previous work, the magnitude of precipitation change is considerably smaller (regardless of the inclusion of indirect effects), highlighting the need for improved understanding and simulation of dust-rainfall responses in order to better understand the role of dust in shaping past and future climates.

Acknowledgments

This work was supported by National Science Foundation Award 1602956. We thank Marco Gaetani, Francesco Pausata, Cheng Zhou, and Allison Steiner for helpful discussion. We also thank Ron Miller and one anonymous reviewer for their insightful and constructive comments. We acknowledge high-performance computing support from Cheyenne (doi:10.5065/D6RX99HX) provided by NCAR's Computational and Information Systems Laboratory, sponsored by the National Science Foundation. This research was supported in part through computational resources and services provided by Advanced Research Computing at the University of Michigan, Ann Arbor. Data link available at https://github.com/alexjt28.

References

Bartlein, P. J., Harrison, S. P., Brewer, S., Connor, S., Davis, B. A. S., Gajewski, K., et al.

(2011). Pollen-based continental climate reconstructions at 6 and 21 ka: a global synthesis. *Climate Dynamics, 37*, 775–802. https://doi.org/10.1007/s00382-010-0904-1

Boos, W. R., & Korty, R. L. (2016). Regional energy budget control of the intertropical convergence zone and application to mid-Holocene rainfall. *Nature Geoscience, 9*(12), 892–897. https://doi.org/10.1038/ngeo2833

Braconnot, P., Joussaume, S., Marti, O., & de Noblet, N. (1999). Synergistic feedbacks from ocean and vegetation on the African monsoon response to mid-Holocene insolation. *Geophysical Research Letters, 26*, 2481-2484. https://doi.org/10.1029/1999GL006047

Braconnot, P., Harrison, S. P., Otto-Bliesner, B., Abe-Ouchi, A., Jungclaus, J., & Peterschmitt, J.-Y. (2011). The Paleoclimate Modeling Intercomparison Project contribution to CMIP5. *CLIVAR Exchanges, 56*(16–2), 15-19. http://www.clivar.org/sites/default/files/documents/Exchanges56.pdf

Bretherton, C. S. (2015). Insights into low-latitude cloud feedbacks from high-resolution models. *Philosophical Transactions of the Royal Society A, 373*(2054), 1-19. https://doi.org/10.1098/rsta.2014.0415

Brostrom, A., Coe, M., Harrison, S. P., Gallimore, R., Kutzbach, J. E., Foley, J., et al. (1998). Land surface feedbacks and palaeomonsoons in northern Africa. *Geophysical Research Letters, 25*(19), 3615–3618. https://doi.org/10.1029/98GL02804

Brovkin, V., Claussen, M., Petoukhov, V., & Ganopolski, A. (1998). On the stability of the atmosphere-vegetation system in the Sahara/Sahel region. *Journal of Geophysical Research, 103*(D24), 31,613-31,624. https://doi.org/10.1029/1998JD200006

Charney, J. G. (1975). Dynamics of deserts and drought in the Sahel. *Quarterly Journal of the Royal Meteorological Society, 101*(428), 193–202.

Charney, J., Stone, P. H., & Quirk, W. J. (1975). Drought in the Sahara: A Biogeophysical Feedback Mechanism. *Science, 187*(4175), 434–435. https://doi.org/10.1126/science.187.4175.434

Claussen, M., & Gayler, V. (1997). The Greening of the Sahara during the Mid-Holocene: Results of an Interactive Atmosphere-Biome. *Global Ecology and Biogeography Letters, 6*(5), 369–377. https://doi.org/10.2307/2997337

Claussen, M., Kubatzki, C., Brovkin, V., Ganopolski, A., Hoelzmann, P., & Pachur, H.-J. (1999). Simulation of an abrupt change in Saharan vegetation in the mid-Holocene. *Geophysical Research Letters, 26*(14), 2037–2040. https://doi.org/10.1029/1999GL900494

Colman, R. (2003). A comparison of climate feedbacks in general circulation models. *Climate Dynamics, 20*(7–8), 865–873. https://doi.org/10.1007/s00382-003-0310-z

Conley, A. J., Lamarque, J. F., Vitt, F., Collins, W. D., & Kiehl, J. (2013). PORT, a CESM tool for the diagnosis of radiative forcing. *Geoscientific Model Development, 6*(2), 469–476. https://doi.org/10.5194/gmd-6-469-2013

Davies, F. J., Renssen, H., Blaschek, M., & Muschitiello, F. (2015). The impact of Sahara desertification on arctic cooling during the Holocene. *Climate of the Past, 11*(3), 571–586. https://doi.org/10.5194/cp-11-571-2015

deMenocal, P. (1995). Plio-Pleistocene African climate. *Science, 270*, 53-59.

deMenocal, P., Ortiz, J., Guilderson, T., Adkins, J., Sarnthein, M., Baker, L., & Yarusinsky, M. (2000). Abrupt onset and termination of the African Humid Period: Rapid climate responses to gradual insolation forcing. *Quaternary Science Reviews, 19*, 347–361. https://doi.org/10. 1016/S0277-3791(99)00081-5

DeMott, P. J., Sassen, K., Poellot, M. R., Baumgardner, D., Rogers, D. C., Brooks, S. D., et al. (2003). African dust aerosols as atmospheric ice nuclei. *Geophysical Research Letters, 30*(14), 1732. https://doi.org/10.1029/2003GL017410

Egerer, S., Claussen, M., Reick, C., & Stanelle, T. (2016). The link between marine sediment records and changes in Holocene Saharan landscape: Simulating the dust cycle. *Climate of the Past, 12*, 1009–1027. https://doi.org/10.5194/cp-12-1009-2016

Eltahir, E. A. B. (1998). A soil moisture-rainfall feedback mechanism 1. Theory and observations. *Water Resources Research, 34*(4), 765–776. https://doi.org/10.1029/97WR03499

Evan, A. T., Flamant, C., Gaetani, M., & Guichard, F. (2016). The past, present and future of African dust. *Nature, 531*(7595), 493–495. https://doi.org/10.1038/nature17149

Forbes, R., Tompkins, A. M., & Untch, A. (2011). A new prognostic bulk microphysics scheme for the IFS. *ECMWF Technical Memorandum*. (No. 649). Reading, UK: European Centre for Medium-Range Weather Forecasts.

Gaetani, M., Messori, G., Zhang, Q., Flamant, C., & Pausata, F. S. R. (2017). Understanding the mechanisms behind the northward extension of the West African Monsoon during the Mid-Holocene. *Journal of Climate, 30*, 7621–7642. https://doi.org/10.1175/JCLI-D-16-0299.1

Gent P. R., Danabasoglu, G., Donner, L. J., Holland, M. M., Hunke, E. C., Jayne, S. R., et al. (2011). The Community Climate System Model Version 4. *Journal of Climate, 24*, 4973–4991. https://doi.org/10.1175/2011JCLI4083.1

Ghan, S. J., Liu, X., Easter, R. C., Zaveri, R., Rasch, P. J., & Yoon, J. (2012). Toward a minimal representation of aerosols in climate models: Comparative decomposition of aerosol direct, semidirect, and indirect radiative forcing. *Journal of Climate, 25*, 6461–6476. https://doi.org/10.1175/JCLI-D-11-00650.1

Ghan, S. J., Smith, S. J., Wang, M., Zhang, K., Pringle, K., Carslaw, K., et al. (2013). A simple model of global aerosol indirect effects. *Journal of Geophysical Research: Atmospheres, 118*, 6688–6707. https://doi.org/10.1002/jgrd.50567

Grassl, H. (1975). Albedo reduction and radiative heating of clouds by absorbing aerosol particles. *Beitr. Phys. Atmos., 48*, 199-209.

Hazeleger, W., Wang, X., Severijns, C., Ştefănescu, S., Bintanja, R., Sterl, A., et al. (2012). EC-Earth V2.2: description and validation of a new seamless earth system prediction model. *Climate Dynamics, 39*(11), 2611–2629. https://doi.org/10.1007/s00382-011-1228-5

Hoelzmann, P., Jolly, D., Harrison, S. P., Laarif, F., Bonnefille, R., & Pachur, H.-J. (1998). Mid-Holocene land-surface conditions in northern Africa and the Arabian peninsula: A data

set for the analysis of biogeophysical feedbacks in the climate system. *Global Biogeochemical Cycles*, *12*(1), 35–51. https://doi.org/10.1029/97GB02733

Hoose, C., Lohmann, U., Erdin, R., & Tegen, I. (2008). The global influence of dust mineralogical composition on heterogeneous ice nucleation in mixed-phase clouds. *Environmental Research Letters*, *3*(025003), 1-14 https://doi.org/10.1088/1748-9326/3/2/025003

Hopcroft, P. O., & Valdes, P. J. (2018). On the role of dust-climate feedbacks during the mid-Holocene. *Geophysical Research Letters*. https://doi.org/10.1029/2018GL080483

Huang, J., Zhang, C., & Prospero, J. M. (2009). African aerosol and large-scale precipitation variability over West Africa. *Environmental Research Letters*, *4*, 1–8. https://doi.org/10.1088/1748-9326/4/1/015006

Huang, H., Gu, Y., Xue, Y., Jiang, J., & Zhao, B. (2018). Assessing aerosol indirect effect on clouds and regional climate of East/South Asia and West Africa using NCEP GFS. *Climate Dynamics*. https://doi.org/10.1007/s00382-018-4476-9

Hurrell, J. W., Hack, J. J., Shea, D., Caron, J. M., & Rosinski, J. (2008). A new sea surface temperature and sea ice boundary dataset for the community atmosphere model. *Journal of Climate*, *21*(19), 5145-5153. https://doi.org/10.1175/2008JCLI2292.1

Jolly, D., Prentice, I. C., Bonnefille, R., Ballouche, A., Bengo, M., Brenac, P., et al. (1998). Biome reconstruction from pollen and plant macrofossil data for Africa and the Arabian peninsula at 0 and 6000 years. *Journal of Biogeography*, *25*(6), 1007–1027. https://doi.org/10.1046/j.1365-2699.1998.00238.x

Joussaume, S., Taylor, K. E., Braconnot, P., Mitchell, J. F. B., Kutzbach, J. E., Harrison, S. P., et al. (1999). Monsoon changes for 6000 years ago: Results of 18 simulations from the Paleoclimate Modeling Intercomparison Project (PMIP). *Geophysical Research Letters*, *26*(7), 859–862. https://doi.org/10.1029/1999GL900126

Knorr, W., & Schnitzler, K. (2006). Enhanced albedo feedback in North Africa from possible combined vegetation and soil-formation processes. *Climate Dynamics*, *26*, 55–63. https://doi.org/10.1007/s00382-005-0073-9

Kutzbach, J. E. (1981). Monsoon climate of the early Holocene: Climate experiment with the earth's orbital parameters for 9000 years ago. *Science*, *214*(4516), 59–61.

Levis, S., Bonan, G. B., & Bonfils, C. (2004). Soil feedback drives the mid-Holocene North African monsoon northward in fully coupled CCSM2 simulations with a dynamic vegetation model. *Climate Dynamics*, *23*, 791–802. https://doi.org/10.1007/s00382-004-0477-y

Lin, L., Xu, Y., Wang, Z., Diao, C., Dong, W., & Xie, S.-P. (2018). Changes in extreme rainfall over India and China attributed to regional aerosol-cloud interaction during the late 20th century rapid industrialization. *Geophysical Research Letters*, *45*, 1–9. https://doi.org/10.1029/2018GL078308

Madec, G., and the NEMO Team. (2008). NEMO ocean engine. *Note du Pôle de modélisation de*

Institut Pierre-Simon Laplace. (No. 27). Paris, France: Institut Pierre-Simon Laplace. Retrieved from https://www.nemo-ocean.eu/wp-content/uploads/NEMO_book.pdf

McGee, D., DeMenocal, P. B., Winckler, G., Stuut, J. B. W., & Bradtmiller, L. I. (2013). The magnitude, timing and abruptness of changes in North African dust deposition over the last 20,000 yr. *Earth and Planetary Science Letters, 371–372*, 163–176. https://doi.org/10.1016/j.epsl.2013.03.054

Messori, G., Gaetani, M., Zhang, Q., Zhang, Q., & Pausata, F. S. R. (2018). The water cycle of the mid-Holocene West African Monsoon: The role of vegetation and dust emission changes. *International Journal of Climatology*, 1-13. https://doi.org/10.1002/joc.5924

Miller, R. L., Tegen, I., & Perlwitz, J. (2004a). Surface radiative forcing by soil dust aerosols and the hydrologic cycle. *Journal of Geophysical Research: Atmospheres*, *109*(D04203), 1-24. https://doi.org/10.1029/2003JD004085

Miller, R. L., Perlwitz, J., & Tegen, I. (2004b). Modeling Arabian dust mobilization during the Asian summer monsoon: The effect of prescribed versus calculated SST. *Geophysical Research Letters*, *31*(22), 1–4. https://doi.org/10.1029/2004GL020669

Miller, R. L., Knippertz, P., Pérez García-Pando, C., Perlwitz, J. P., & Tegen, I. (2014). Impact of Dust Radiative Forcing upon Climate. In P. Knippertz & J.-B. W. Stuut (Eds.), *Mineral Dust: A Key Player in the Earth System* (pp. 327–357). Dordrecht: Springer Netherlands. https://doi.org/10.1007/978-94-017-8978-3_13

Myhre, G., D. Shindell, F.-M., Bréon, W., Collins, J., Fuglestvedt, J., Huang, D., et al. (2013). Anthropogenic and Natural Radiative Forcing. In T.F. Stocker, D. Qin, G.-K. Plattner, M. Tignor, S. K. Allen, J.Boschung, et al. (Eds.), *Climate Change 2013: The Physical Science Basis. Contribution of Working Group I to the Fifth Assessment Report of the Intergovernmental Panel on Climate Change* (pp. 659-740). Cambridge, UK and New York: Cambridge University Press.

Neale, R. B., Chen, C.-C., Gettelman, A., Lauritzen, P. H., Park, S., Williamson, D. L., et al. (2012). *Description of the NCAR Community Atmosphere Model* (CAM5.0) (NCAR/TN-486+STR). Boulder, CO: National Center for Atmospheric Research.

Oleson, K. W., Lawrence, D. M., Bonan, G. B., Flanner, M. G., Kluzek, E., Lawrence, P. J. et al. (2010). *Technical description of version 4.0 of the Community Land Model* (CLM) (NCAR/TN-478+STR). Boulder, CO: National Center for Atmospheric Research.

Patricola, C. M., & Cook, K. H. (2007). Dynamics of the West African monsoon under mid-Holocene precessional forcing: Regional climate model simulations. *Journal of Climate, 20*, 694-716. https://doi.org/10.1175/JCLI4013.1.

Pausata, F. S. R., Messori, G., & Zhang, Q. (2016). Impacts of dust reduction on the northward expansion of the African monsoon during the Green Sahara period. *Earth and Planetary Science Letters, 434*, 298–307. https://doi.org/10.1016/j.epsl.2015.11.049

Perez-Sanz, A., Li, G., González-Sampériz, P., & Harrison, S. P. (2014). Evaluation of modern and mid-Holocene seasonal precipitation of the Mediterranean and northern Africa in the CMIP5 simulations. *Climate of the Past*, *10*(2), 551–568. https://doi.org/10.5194/cp-10-

551-2014
Perlwitz, J., & Miller, R. L. (2010). Cloud cover increase with increasing aerosol absorptivity: A counterexample to the conventional semidirect aerosol effect. *Journal of Geophysical Research Atmospheres*, *115*(8), 1–23. https://doi.org/10.1029/2009JD012637
Rosenfeld, D., Rudich, Y., & Lahav, R. (2001). Desert dust suppressing precipitation: A possible desertification feedback loop. *Proceedings of the National Academy of Sciences of the United States of America*, *98*(11), 5975–5980. https://doi.org/10.1073/pnas.101122798
Sagoo, N., & Storelvmo, T. (2017). Testing the sensitivity of past climates to the indirect effects of dust. *Geophysical Research Letters*, *44*, 5807–5817. https://doi.org/10.1002/2017GL072584
Sassen, K., DeMott, P. J., Prospero, J. M., & Poellot, M. R. (2003). Saharan dust storms and indirect aerosol effects on clouds: CRYSTAL-FACE results. *Geophysical Research Letters*, *30*(12), 1633. https://doi.org/10.1029/2003GL017371
Shanahan, T. M., Mckay, N. P., Hughen, K. A., Overpeck, J. T., Otto-Bliesner, B., Heil, C. W., et al. (2015). The time-transgressive termination of the African Humid Period. *Nature Geoscience*, *8*, 140–144. https://doi.org/10.1038/NGEO2329
Skinner, C. B., & Poulsen, C. J. (2016). The role of fall season tropical plumes in enhancing Saharan rainfall during the African Humid Period. *Geophysical Research Letters*, *43*, 349–358. https://doi.org/10.1002/2015GL066318
Solmon, F., Elguindi, N., & Mallet, M. (2012). Radiative and climatic effects of dust over West Africa, as simulated by a regional climate model. *Climate Research*, *52*(1), 97–113. https://doi.org/10.3354/cr01039
Strong, J. D. O., Vecchi, G. A., & Ginoux, P. (2015). The response of the tropical Atlantic and West African climate to Saharan dust in a fully coupled GCM. *Journal of Climate*, *28*(18), 7071–7092. https://doi.org/10.1175/JCLI-D-14-00797.1
Taylor, K. E., Stouffer, R. J., & Meehl, G. A. (2012). An overview of CMIP5 and the experiment design. *Bulletin of the American Meteorological Society*, *93*(4), 485–498. https://doi.org/10.1175/BAMS-D-11-00094.1
Tierney, J. E., Pausata, F. S. R., & deMenocal, P. B. (2017). Rainfall regimes of the Green Sahara. *Science Advances*, *3*, 1–9. https://doi.org/10.1126/sciadv.1601503
Tilmes, S., Lamarque, J. F., Emmons, L. K., Kinnison, D. E., Ma, P. L., Liu, X., et al. (2015). Description and evaluation of tropospheric chemistry and aerosols in the Community Earth System Model (CESM1.2). *Geoscientific Model Development*, *8*, 1395–1426. https://doi.org/10.5194/gmd-8-1395-2015
Tjallingii, R., Claussen, M., Stuut, J. B. W., Fohlmeister, J., Jahn, A., Bickert, T., et al. (2008). Coherent high-and low-latitude control of the northwest African hydrological balance. *Nature Geoscience*, *1*, 670–675. https://doi.org/10.1038/ngeo289
Tuenter, E., Weber, S. L., Hilgen, F. J., & Lourens, L. J. (2007). Simulating sub-Milankovitch climate variations associated with vegetation dynamics. *Climate of the Past*, *3*, 169–180. https://doi.org/10.5194/cp-3-169-2007

Vamborg, F. S. E., Brovkin, V., & Claussen, M. (2014). Background albedo dynamics improve simulated precipitation variability in the Sahel region. *Earth System Dynamics*, *5*, 89–101. https://doi.org/10.5194/esd-5-89-2014

Vergara-Temprado, J., Murray, B. J., Wilson, T. W., O'Sullivan, D., Browse, J., Pringle, K. J., et al. (2017). Contribution of feldspar and marine organic aerosols to global ice nucleating particle concentrations. *Atmospheric Chemistry and Physics*, *17*(5), 3637–3658. https://doi.org/10.5194/acp-17-3637-2017

Williams, R. H., McGee, D., Kinsley, C. W., Ridley, D. A., Hu, S., Fedorov, A., et al. (2016). Glacial to Holocene changes in trans-Atlantic Saharan dust transport and dust-climate feedbacks. *Science Advances*, *2*, 1–11. https://doi.org/10.1126/sciadv.1600445

Xie, S., Ma, H. Y., Boyle, J. S., Klein, S. A., & Zhang, Y. (2012). On the correspondence between short- and long-time-scale systematic errors in CAM4/CAM5 for the year of tropical convection. *Journal of Climate*, *25*(22), 7937–7955. https://doi.org/10.1175/JCLI-D-12-00134.1

Xie, X., Zhang, H., Liu, X., Peng, Y., & Liu, Y. (2017). New cloud parameterization with relative dispersion in CAM5.1: model evaluation and impacts on aerosol indirect effects. *Atmospheric Chemistry and Physics*, *17*, 5877-5892. https://doi.org/10.5194/acp-17-5877-2017

Yoshioka, M., Mahowald, N. M., Conley, A. J., Collins, W. D., Fillmore, D. W., Zender, C. S., & Coleman, D. B. (2007). Impact of desert dust radiative forcing on Sahel precipitation: Relative importance of dust compared to sea surface temperature variations, vegetation changes, and greenhouse gas warming. *Journal of Climate*, *20*(8), 1445–1467. https://doi.org/10.1175/JCLI4056.1

Yu, M., Wang, G., & Pal, J. S. (2016). Effects of vegetation feedback on future climate change over West Africa. *Climate Dynamics*, *46*(11–12), 3669–3688. https://doi.org/10.1007/s00382-015-2795-7

Zender, C. S. (2003). Mineral Dust Entrainment and Deposition (DEAD) model: Description and 1990s dust climatology. *Journal of Geophysical Research*, *108*(D14), 4416. https://doi.org/10.1029/2002JD002775

Zhang, Z., Ramstein, G., Schuster, M., Li, C., Contoux, C., & Yan, Q. (2014). Aridification of the Sahara desert caused by Tethys Sea shrinkage during the Late Miocene. *Nature*, *513*(7518), 401–404. https://doi.org/10.1038/nature13705

Zhu, Z., Piao, S., Myneni, R. B., Huang, M., Zeng, Z., Canadell, J. G., et al. (2016). Greening of the Earth and its drivers. *Nature Climate Change*, *6*(8), 791–795. https://doi.org/10.1038/nclimate3004

Figure 1. JJAS differences between *MH Control* and *MH HighDust* in a) dust AOD, b) net surface shortwave radiation flux diagnosed from offline radiation calculations, c) 2-m air temperature, d) profile of convective cloud cover averaged over the Sahara, e) convective rainfall, and f) total rainfall. In spatial maps, dashed boxes signify Saharan (upper) and Sahel (lower in e-f) extent used to calculate percent changes noted in left corner(s) of each panel. Numbers in atmospheric profile represent the percent change in cloud fraction at specific atmospheric levels (850 hPa, 500 hPa, and 200 hPa). Stippling in spatial maps and shading in the atmospheric profile indicate statistically significant differences at the 95% confidence level.

Figure 2. JJAS Saharan-average atmospheric profiles for a) in-cloud ice crystal number concentration, b) in-cloud liquid droplet number concentration, c) in-cloud ice crystal radius, d) in-cloud liquid droplet radius, e) stratus cloud fraction, and f) spatial map of stratiform rainfall difference between *MH Control* and *MH HighDust*. Atmospheric profile and spatial map description same as Figure 1. "In-cloud" variables are calculated by dividing the specified cloud variable (e.g., ice crystal number concentration) by its fractional occurrence. Calculated differences for profile levels are shown as follows: a) 200 hPa, b) 750 hPa and 925 hPa, c) 200 hPa, d) 750 hPa and 925 hPa, and e) 200 hPa and 850 hPa.

Table 1. List of Simulations and Boundary Conditions, Northern WAM Limits (°N), and JJAS Dust Aerosol Optical Depth and Rainfall (mm day^{-1})

Simulation	Orbital forcing[a]	Vegetation[a]	Soil albedo[a]	Mobilizes Saharan dust?	Northern limit of West African Monsoon	Dust aerosol optical depth[b]	Total rainfall[b]	Convective rainfall[b]	Stratiform rainfall[b]
PI Control	PI	PI	PI	Yes	19.3	**0.43** 0.30	**0.26** 4.41	**0.22** 3.73	**0.04** 0.68
MH Control	MH	MH	MH	No	28.7	**0.02** 0.01	**2.54** 7.62	**2.26** 5.90	**0.28** 1.72
MH HighDust	MH	MH	MH	Yes	27.8	**0.96** 0.24	**2.27** 7.44	**1.95** 5.47	**0.32** 1.97
MH DesertVeg	MH	PI	MH	No	25.9	**0.03** 0.02	**1.35** 6.54	**1.21** 5.36	**0.14** 1.18

MH DesertSoil	MH	MH	PI	No	28.7	**0.02** 0.01	**2.39** 7.51	**2.15** 5.82	**0.24** 1.69
MH Orbital	MH	PI	PI	Yes	22.1	**0.48** 0.24	**0.62** 5.50	**0.54** 4.48	**0.08** 1.02

[a]PI=Preindustrial, MH=Mid-Holocene. [b]Averages for Sahara (**bold** text) and Sahel (plain text).

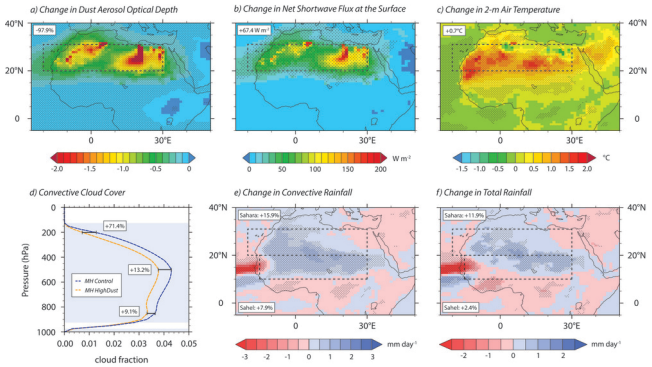

2018GL081225-f01-z-.jpg

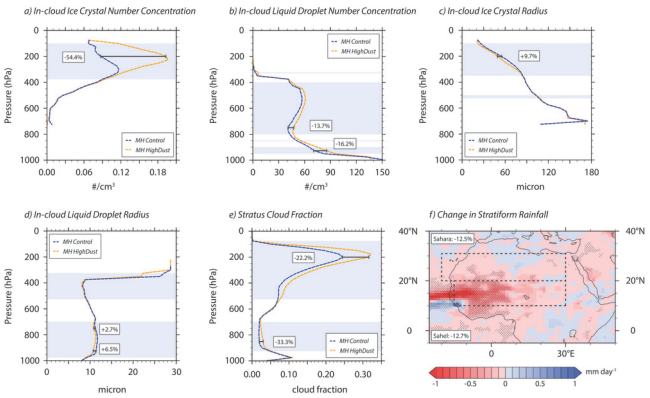

2018GL081225-f02-z-.jpg